Advanced Physical Research
Vol.3, No.2, 2021, pp.59-67

STUDY OF CATION DISTRIBUTION EFFECT ON Cu AND Cr DOPED $MgFe_2O_4$ SPINEL FERRITE

B. Enkhmend, I. Khishigdemberel, N. Jargalan, D. Sangaa

Institute of Physics and Technology, Mongolian Academy of Sciences, Ulaanbaatar, Mongolia

Abstract. In this work, we have carried out a comprehensive study on the impact of cation distribution towards tuning the structural and molecular parameters and finally optimizing the heating efficiency of the nanoparticles for magnetic hyperthermia application. Nanomagnetic spinel ferrite samples with the general formula $Mg_{0.4}Cu_{0.6}CrxFe_{2-x}O_4$ (x = 0.0, 0.2, 0.5, 1.0) which synthesized by sol-gel method, has been studied by different methods. Characteristics structural parameters have been examined from X-ray diffraction spectra by employing standard Rietveld refinement techniques. The vibrational study was achieved using Fourier Transform-InfraRed (FT-IR) spectroscopy. Cation migration in the unit cell is confirmed from the XRD peak intensity and FTIR study. The shifting of bands toward high frequency is attributed to the decrease in the unit cell dimension as confirmed from XRD results and substitution of lighter cations Cr^{3+} for Fe^{3+} in the system. The heat generation ability of the synthesized samples was studied upon exposure to an external alternation magnetic field of 75 kHz and 7.5 kA/m. Specific absorption rate (SAR) of the ferrite samples calculated by calorimetric method.

Keywords: *Ferrite, spinel structure, x-ray diffraction, Rietveld analysis, cation distribution and SAR.*

Corresponding Author: *B. Enkhmend, Institute of Physics and Technology, Mongolian Academy of Sciences, 13330 Ulaanbaatar, Mongolia, e-mail: enkhmendb@mas.ac.mn*

Received: *30 June 2021;* ***Accepted:*** *14 July 2021;* ***Published:*** *20 August 2021.*

1. Introduction

Although significant advances have been made by nanoparticles for the applications in magnetic hyperthermia, the optimization and related mechanism of heating efficiency is nevertheless a challenge. The cation distribution effect plays a major role in the heat generation ability for the spinel ferrite. The spinel ferrites with general formula MFe_2O_4have been used in many industrial applications. By adjusting the chemical identity of the M^{2+} cation, the magnetic configurations of MFe_2O_4 are tunable to provide a wide range of magnetic properties (O'Handley, 2000). Some of the applications of these materials are in permanent magnets, recording devices, electronic and microwave devices, high frequencies device and catalyst for environment. In addition, magnetic nanoparticles can be utilized for the magnetic hyperthermia treatment of cancer. The magnetic nanoparticles are used as heat generators under an alternating magnetic field.

In ferrites, the magnetic properties are mainly dependent on the type of metal ions and their distribution between the tetrahedral (A) and octahedral (B) sites (Kumar *et al.*, 2017) Spinel ferrites usually contains a crystal structure with the space group, Fd3m, having 56 atoms; 32 are oxygen anions with a close packed cubic structure, and the rest are metal cations: 8 (of 64 available) occupying the tetrahedral (A) sites and 16 (of 32

available) occupying the octahedral (B) sites (Hashim *et al*., 2014). The structural formula for a generic spinel compound MFe_2O_4 can be written as

$$(M_{1-\delta}Fe_{\delta})^{A}[M_{2-\delta}Fe_{2-\delta}]^{B}O_4 \quad (1)$$

where the amounts in $(\ )^A$ and $[\ ]^B$ brackets represent the average occupancy of A sites (tetrahedral) and B sites (octahedral), and δ is the inversion parameter. For a normal spinel, $\delta = 0$, for a fully inverted spinel, $\delta = 1$, and for partially inverted, $0 < \delta < 1$ (Carta *et al*., 2009).

In our previous work (Khishigdemberel *et al*., 2018), heat generation ability of Cu doped $MgFe_2O_4$ferrites were studied. The ferrites showed better heating ability via Cu substitution as highest heating occurred for $Mg_{0.4}Cu_{0.6}Fe_2O_4$ due to their structural and magnetic properties variation. (Kiseleva *et al*., 2018).

Also we studied the effect of the composition on the inversion factor of Cr^{3+}doped $CuFe_2O_4$ materials. As the Fe^{3+} cations are replaced by Cr^{3+} cations, the $CuFe_{2-x}Cr_xO_4$ inversion changes smoothly from 1 to 0 (Plyasova & Minyukova, 2018). So in further study we used Cr^{3+} substitution on $Mg_{0.4}Cu_{0.6}Fe_2O_4$in order to see its heat generation ability dependence on inversion factor.

In the present paper, we report the synthesis of $Mg_{0.4}Cu_{0.6}Cr_xFe_{2-x}O_4$ using sol-gel and its characterization. Change of the inversion factorvia Cr^{3+} substitution is refined by Rietveld refinement. Upon exposure to an external alternation magnetic field of 75 kHz, heat generation ability and specific absorption rate (SAR) materials are measured.

2. Experimental

Sol-gel method was used for preparation of $Mg_{0.4}Cu_{0.6}Cr_xFe_{2-x}O_4$ (x = 0.0, 0.2, 0.5, 1.0) ferrites. The aqueous sol was produced by dissolving stoichiometric mix of iron nitrate$Fe(NO_3)_3 \cdot 9H_2O$ (98.5%), magnesium nitrate $Mg(NO_3)_2 \cdot 6H_2O$ (99%), copper nitrate $Cu(NO_3)_2 \cdot 6H_2O$ (99%) and chromium nitrate $Cr(NO_3)_3 \cdot 9H_2O$ (99%) in deionized water. Citric acid and Ethelyne glycol were added to the sol for the enhancement of nitrates dissolution. The sol was heated at 100^0 C to obtain a gel and dried at 400^0 C. Then the obtained powder was sintered at 900ºC in ambient air for 2h.

Phase analysis of obtained samples were determined by Shimadzu XRD-7000 powder X-ray diffraction (XRD) with CuK_α radiation (λ =1.5406Å). Fourier-transform infrared (FT-IR) spectra were recorded on Shimadzu IR Prestige-21 spectrometer in the range of 4000 cm^{-1} to 400 cm^{-1} wavelengths. Heat generation ability measurements were carried out by special designed device as shown in Fig.1. The coil consists of loops of copper pipe (diameter 1 cm; seven turns) and the copper pipe is cooled by water to keep its temperature constant. The temperature generation of the sample was monitored using an alcohol thermometer. This equipment was calibrated by using a blank sample, without ferrite nanoparticles in the water.

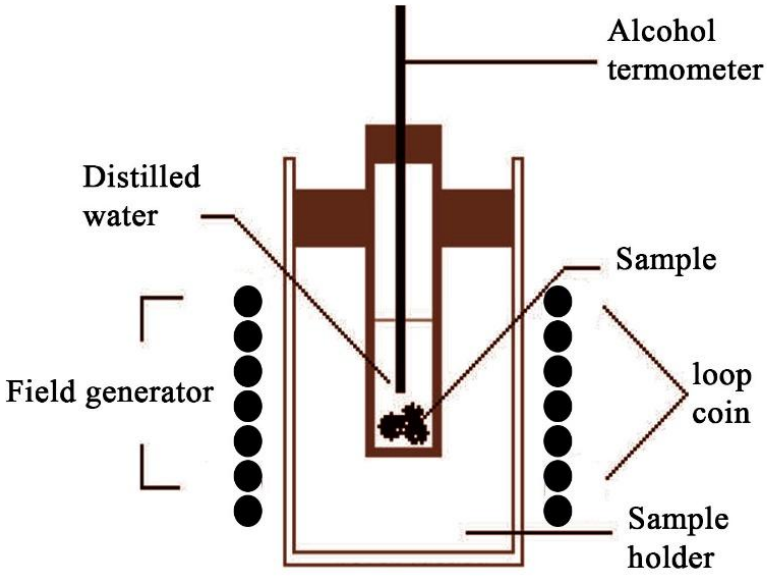

Fig. 1. Specially designed equipment assembly for heat-generation ability measurement

3. Results and discussions

Fig. 2*a* shows the XRD patterns of $Mg_{0.4}Cu_{0.6}Cr_xFe_{2-x}O_4$ (x = 0.0, 0.2, 0.5 and 1.0) ferrites. XRD patterns confirm that the synthesized ferrite powders are well-crystalline single spinel structures. Fig. 2*b* shows a shift of peak (311) at x = 0, 0.2, 0.5 and 1, indicating the lattice parameters variation due to chromium content.

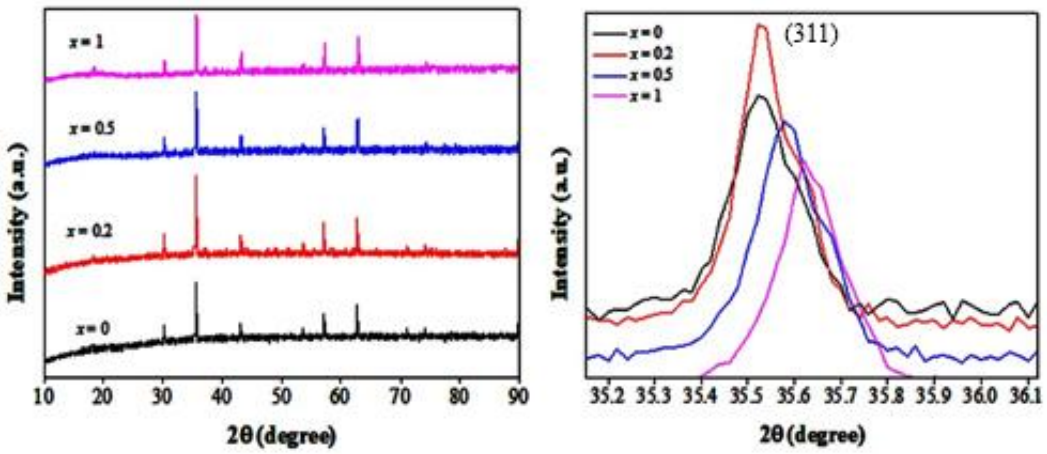

Fig. 2. *a*) XRD patterns, ***b*)** analysis of the (311) peak shift of the $Mg_{0.4}Cu_{0.6}Cr_xFe_{2-x}O_4$(x = 0.0, 0.2, 0.5, 1.0) ferrites

XRD patterns were analyzed using the FullProf suite program which is based on the Rietveld refinement method (Young & Wiles, 1982). The patterns for all the samples refined using the Fd3m space group, and pseudo-Voigt function was utilized with the oxygen positions ($x = y = z = u$) taken as free parameters. The Rietveld refinement of all XRD patterns for $Mg_{0.4}Cu_{0.6}Cr_xFe_{2-x}O_4$ (x = 0.0, 0.2, 0.5, 1.0) ferrites at room temperature

are shown in Fig. 3. The fitting quality of the experimental data is assessed by computing the parameters such as goodness of fit χ^2 and R factors (Kumar *et al*., 2013). These factors and refined values of structural parameters; lattice constant, crystallite size for the samples are tabulated in Table 1.

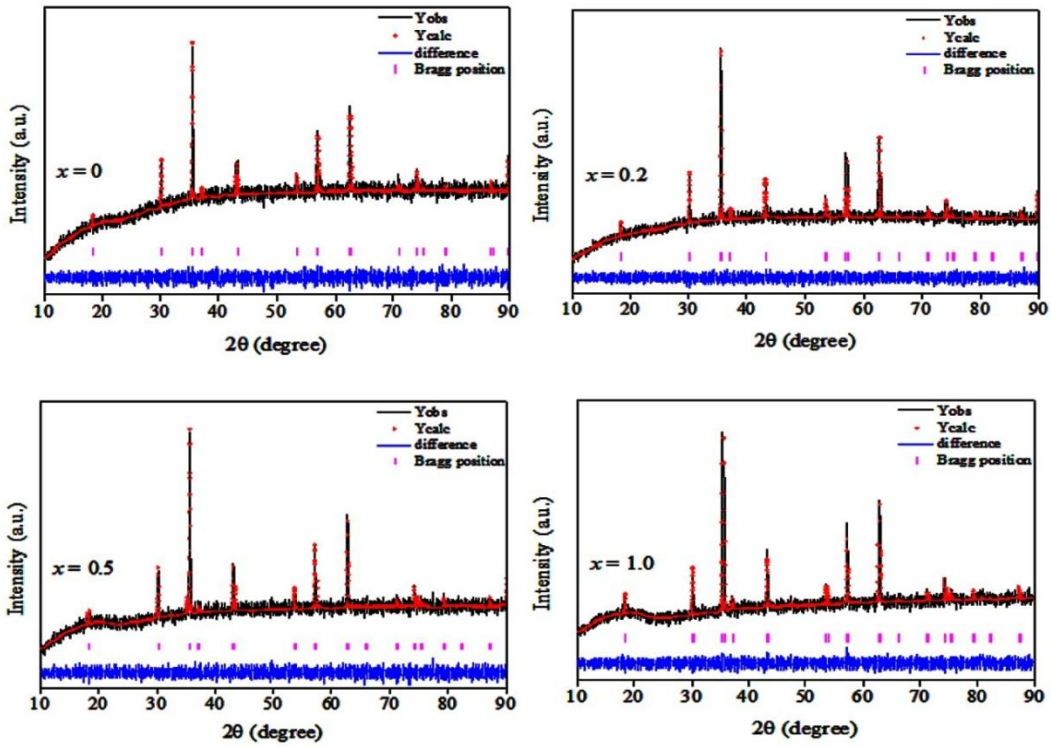

Fig. 3. Rietveld refined XRD patterns of $Mg_{0.4}Cu_{0.6}Cr_xFe_{2-x}O_4$ samples

Table.1. Structural parameters of the $Mg_{0.4}Cu_{0.6}Cr_xFe_{2-x}O_4$ samples estimated from Rietveld refinement: lattice parameter (*a*), crystallite size (D), goodness of fit and cation distribution of spinel $Mg_{0.4}Cu_{0.6}Cr_xFe_{2-x}O_4$ ferrites

x	a_{cub}, Å	D_{XRD} (Å)	Goodness of fit (χ^2)	Cation distribution	
				Tetrahedral (8a) site	Octahedral (16d) site
0.0	8.38073±0.00106	792	1.05	$(Mg_{0.14}Cu_{0.26}Fe_{0.6})_A$	$(Mg_{0.26}Cu_{0.34}Fe_{1.4})_B$
0.2	8.37409±0.00077	887	1.04	$(Mg_{0.15}Cu_{0.28}Fe_{0.57})_A$	$(Mg_{0.25}Cu_{0.32}Fe_{1.23}Cr_{0.2})_B$
0.5	8.36577±0.00125	726	1.10	$(Mg_{0.16}Cu_{0.32}Fe_{0.52})_A$	$(Mg_{0.24}Cu_{0.28}Fe_{0.98}Cr_{0.5})_B$
1.0	8.36046±0.00103	698	1.07	$(Mg_{0.17}Cu_{0.33}Fe_{0.5})_A$	$(Mg_{0.23}Cu_{0.27}Fe_{0.5}Cr_{1.0})_B$

The obtained values lie between 8.3849±0.0012 and 8.2913±0.0003 Å and are found to decrease with the increase of Cr^{3+} content as listed in Table1. Since Cr^{3+} ion have smaller ionic radii (0.64 Å), than those of Fe^{3+} ions (0.645 Å) in the octahedral sites, a partial replacement of the Fe^{3+} ions by the Cr^{3+} ions cause shrinkage of unit cell dimensions, thereby decreasing the lattice parameter (Sirinavas *et al.,* 2016). Similar behavior has been reported for Ni-Al ferrites (Bouhadouza *et al*., 2015) and Ni-Cr ferrites (Hankare *et al.,* 2009). The estimated cation distribution might be explained as follows: in spinel lattice, the radius of the octahedral site is larger than tetrahedral site.

Fig. 4*a* shows that our lattice parameter variation with chromium content obtained by Rietveld refinement confirms that Vegard's law is obeyed for this ferrite system. The crystallite size D_{XRD}, of each sample was evaluated from the reflected diffraction peaks of the Rietveld refined profile using Scherrer's equation (Culity, 1978):

$$D_{XRD} = \frac{k \cdot \lambda}{\beta \cdot cos\theta} \quad (2)$$

where the constant $k = 0.89$, λ is the wavelength of the X-ray radiation ($\lambda = 1.5406$Å), θ is the diffraction angle of the most intensity peak (311) and β is its full width at half maximum (FWHM) in radian.

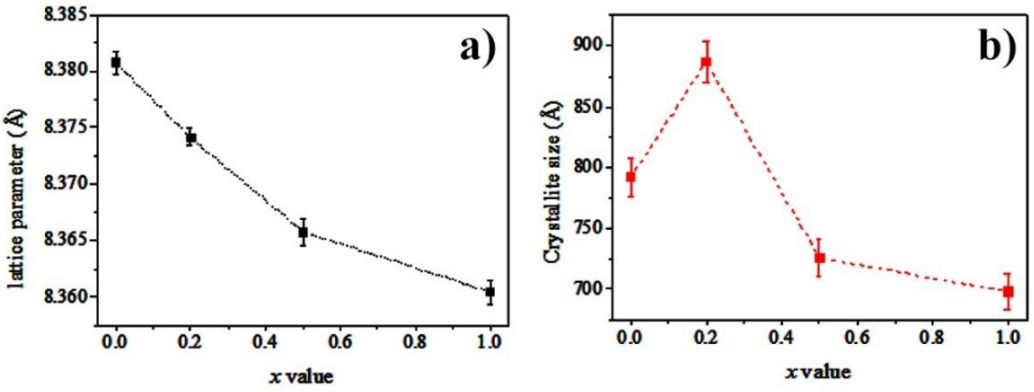

Fig. 4. *a*) Rietveld refined lattice parameter a values *b*) crystallite size of $Mg_{0.4}Cu_{0.6}Cr_xFe_{2-x}O_4$ferrite system

The Rietveld refined cell parameters, sites A and B bond lengths R_A and R_B respectively are shown in Table 2. The systematically decreasing trend of all these parameters with chromium content is consistent with the substitution of cations Fe^{3+} by smaller size Cr^{3+}.

Table 2. Tetrahedral and octahedral vibration frequencies (v_1 and v_2) and force constants (K_T and K_O) of tetrahedral and octahedral sites at room temperature

x	v_1	v_2	$K_T \times 10^5$ (dyne cm^{-1})	$K_O \times 10^5$ (dyne cm^{-1})	Bond length (Å)	
					Tetrahedral (8a) site	Octahedral (16d) site
0.0	571.42	406.50	1.01	0.50	1.9016	2.0461
0.2	579.61	411.32	1.03	0.52	1.9001	2.0445
0.5	594.56	440.25	1.08	0.59	1.8982	2.0425
1.0	606.61	491.36	1.12	0.74	1.8970	2.0412

The IR spectra can give information on the valence states and the different variable modes in the crystal lattice. The room temperature IR spectra for $Mg_{0.4}Cu_{0.6}Cr_xFe_{2-x}O_4$($x$ = 0.0, 0.2, 0.5, 1.0) samples are shown in Fig. 5. Many absorption bands were observed in the range 400–1500 cm^{-1}. The two main common bands of the tetrahedral and octahedral sites are observed in the range (571–606 cm^{-1}) and (406–491 cm^{-1}), respectively (Kawade *et al.*, 2000). These two bands are attributed to the intrinsic stretching vibrations due to the interaction of oxygen atom and cations in the tetrahedral and octahedral complexes, respectively. The shifting of bands toward high frequency is

attributed to the decrease in the unit cell dimension as confirmed from XRD results and substitution of lighter cations Cr^{3+} for Fe^{3+} in the system.

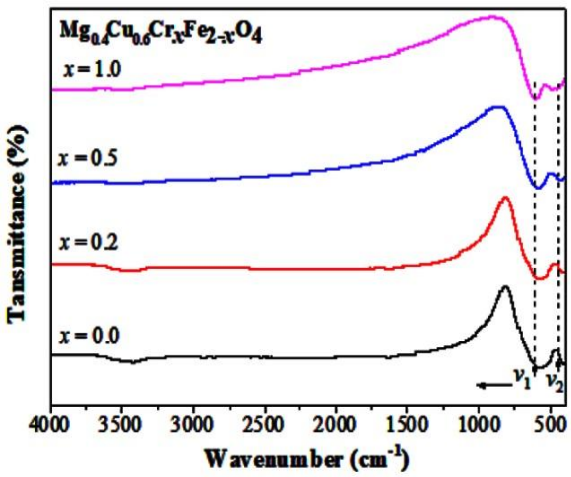

Fig. 5. The IR spectra of$Mg_{0.4}Cu_{0.6}Cr_xFe_{2-x}O_4$ (x = 0.0, 0.2, 0.5 and 1.0) ferrites

It is obvious that the position of the two strong bands are related to the difference in the Fe-O bond lengths at A-sites and B-sites (Table 2). The force constants of the ions at the tetrahedral site (K_T) and octahedral site (K_O) have been calculated using the IR band frequencies ν_1 and ν_2 in the following formula (Zaki & Dawoud, 2010):

$$K = 4\pi^2 c^2 v^2 \mu \quad (3)$$

where c is the light velocity (2.99×108 m/s), ν is the vibration frequency of the sites A and the B, μ is the reduced mass. Table 2 shows variation of K_T and K_O with chromium content.

The variations of force constants K_T and K_O with the corresponding bond lengths R_A and R_B respectively, are shown in Fig. 6. The decreasing trend of both K_T and K_O with R_A and R_B respectively, could be interpreted as due to the fact that it requires less energy to break longer bond lengths than shorter ones (Sabri *et al*., 2016). Similar behavior has been reported for other metal oxides like Ni-Co-Mn ferrites (Kumar *et al*., 2014). If the radius of the substitution ion is smaller than the displaced ion then the bond length decreases. Although the values of the bond length of A-site (R_A) are smaller than those of B-site (R_B), the calculated values of K_T are greater than those of K_O. This is due to the inverse proportionality between the bond length and the force constants (Watawe & Sutar, 2001).

Samples (50 mg) suspended in 1 mL of distilled water were placed at the center of the coil and the applied frequency was 75 kHz. Fig. 7a plots the temperature enhancement from room temperature (ΔT) for $Mg_{0.4}Cu_{0.6}Cr_xFe_{2-x}O_4$ (x = 0.0, 0.2, 0.5, 1.0) ferrites. As seen in graphs, the temperature in the container is elevated rapidly in the first 3 min; thereafter, the temperature increase rate slows down gradually. Generally, the temperature of these samples significantly increased with time in the AC magnetic field. The temperature enhancement of the samples are reached a saturation temperature in 22 min under AC magnetic field. The heat generation ability and the cooling rate in ambient air were equilibrated at the elevated temperature.

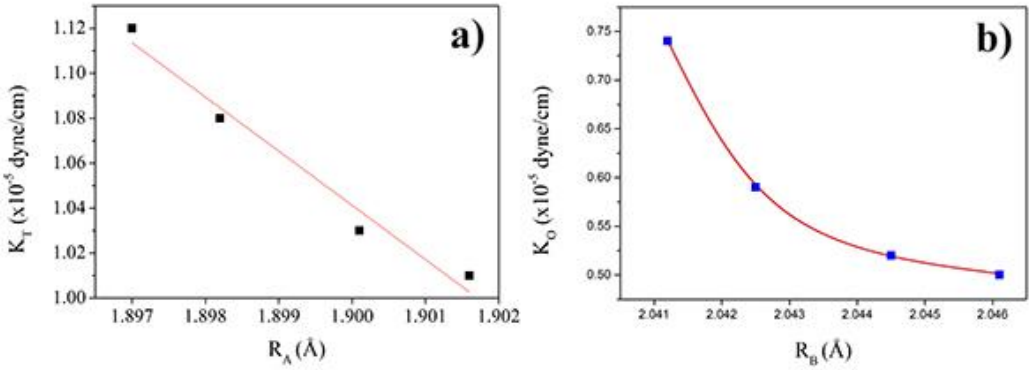

Fig. 6. Force constants *a*) K_T in tetrahedral site, *b*) K_O in octahedral site vs bond lengths R_A and R_B

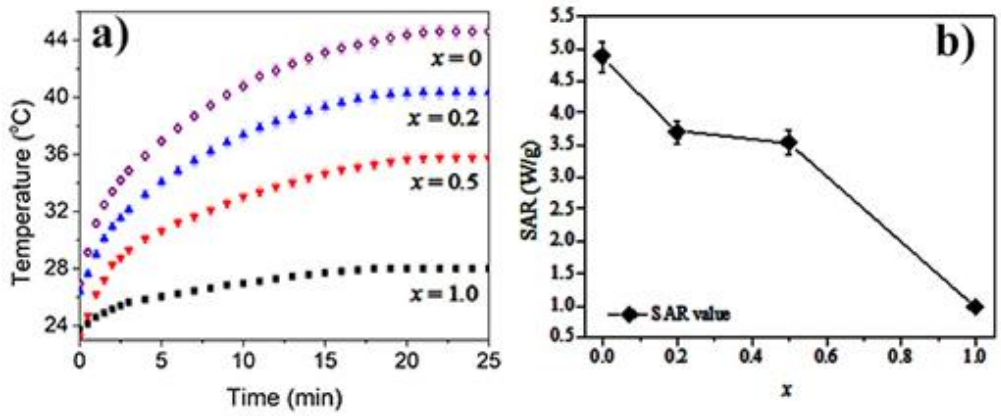

Fig. 7. *a*) Time-dependent temperature enhancement curves *b*) Specific Absorption Rate values of the samples with different concentration of substitution

Specific absorption rate (SAR) values or the heat-generation ability of these samples are calculated referring to Hilger's technique (Hilger *et al*., 2002).

$$SAR = c(\Delta T/\Delta t) \quad (5)$$

where c is specific heat capacity (found from the amount of samples in the solution and heat capacities) and ($\Delta T/\Delta t$) is the initial slope of the curve of temperature versus heating time.

The nanoparticle heating processes in AC magnetic fields could be theoretically explained by ohmic, magnetic hysteretic (Vallejo-Fernandez *et al*., 2013; Mamiya, 2013), and relaxation losses (Mozafari *et al*., 2014). The most evident energy loss mechanisms are related to the magnetic hysteresis loss, Neel and Brownian relaxations in the case of single domain magnetic nanoparticles (Rosensweig, 2002).

Table 3. Calculated SAR values of the as-synthesized samples. The carrier liquid is water, and weight of the powder sample is 50 mg

Sample	SAR value (W/g)
$Mg_{0.4}Cu_{0.6}Fe_2O_4$	4.88(24)
$Mg_{0.4}Cu_{0.6}Cr_{0.2}Fe_{1.8}O_4$	3.70(18)
$Mg_{0.4}Cu_{0.6}Cr_{0.5}Fe_{1.5}O_4$	3.54(17)
$Mg_{0.4}Cu_{0.6}Cr_1Fe_1O_4$	0.98(05)

The obtained values of SAR are listed in Table 3 and shown in Fig. 7. Both saturation temperature and SAR values are decreased with Cr^{3+} dopants. From XRD results, it was foundthat Cr^{3+} ions have strong site preference for B sites. The increase of Cr content led to minimize the number of Fe^{3+} ions at these sites and consequently the net magnetic moment decreased, which may result decreases of the magnetization saturation. Since heat generation ability of magnetic materials are strongly related to these magnetic properties, we assume that substitution of Cr^{3+} ions may decreased magnetic property of $Mg_{0.4}Cu_{0.6}Cr_xFe_{2-x}O_4$ ferrite and therefore decreases heating ability.

4. Conclusion

Polycrystalline $Mg_{0.4}Cu_{0.6}Cr_xFe_{2-x}O_4$(x = 0.0, 0.2, 0.5 and 1.0) ferrites samples have been synthesized by sol-gel method. XRD analysis revealed the prepared samples are cubic spinel with single phase in all concentration, this confirms that the Cr^{3+} ions replaced the Fe^{3+} ions without distortion of the cubic symmetry of the host magnesium ferrite. The lattice parameters are found to decrease with Cr substitution due to smaller ionic radii of Cr^{3+} ions.

The FT-IR spectra indicate two main absorption bands, (571–606 cm-1) fortetrahedral (A) sites and (406–491 cm-1) for octahedral [B] sites, thus confirming the single phase spinel structure.Heat generation ability of pure $Mg_{0.4}Cu_{0.6}Fe_2O_4$ ferrite material was high as saturation temperature is reached 45℃ in low frequency of 75 kHz. Substitution of Cr^{3+}led to a decrease in heat generation ability due to its lack of magnetic behavior.

References

Bouhadouza, N., Rais, A., Kaoua, S., Moreau, M., Taibi, K., Addou, A. (2015). Structural and Vibrational Studies of $NiAl_xFe_{2-x}O_4$ Ferrites ($0 \leq x \leq 1$). *Ceramic International*, 41, 11687-11692.

Carta, D., Casula, M.F., Falqui, A., Loche, D., Mountjoy, G., Sangregorio, C., Corrias, A. (2009). A structural and magnetic investigation of the inversion degree in ferrite nanocrystals MFe_2O_4 (M = Mn, Co, Ni). *The Journal of Physical Chemistry C*, 113, 8606-8615.

Culity, B. (1978). Elements of X-ray Diffraction, vol. second ed., no. Addison-Wesley Series.

Hankare, P.P., Vader, V.,T., Patil, N.M., Jadhav, S.D., Sankpal, U.B., Kadam, M.R., Chougule, B.K., Gajbhiye, N.S. (2009). Synthesis, characterization and studies on magnetic and electrical properties of Mg ferrite with Cr substitution. *Materials Chemistry and Physics*, 113, 233-238.

Hashim, M, Meena, S.S., Kotnala, R.K., Shirsath, S.E., Roy, A.S., Parveen, A., Bhatt, P., Kumar, S., Jotania, R.B., Kumar, R., Alimuddin. (2014). Study of structural, electrical and magnetic properties of Cr doped Ni-Mg ferrite nanoparticle. *Journal of Alloys and Compounds*, 602, 150-156.

Hilger, H., Fruhauf, K., Andra, W., (2002). Heating potential of iron oxides for therapeutic purposes in interventional radiology. *Academic Radiology*, 9, 198.

Kawade, V.B., Bichile, G.K., Jadhav, K.M., (2000). X-ray and infrared studies of chromium substituted magnesium ferrite. *Materials Letters*, 42, 33-37.

Khishigdemberel, I., Uyanga, E., Hirazawa, H., Sangaa, D. (2018). Influence of Cu dope on the structural behavior of $MgFe_2O_4$ at various temperatures. *Physica B: Condensed Matter*, 544, 73-78.

Kiseleva, T., Kabanov, V., Ilyushin, A., Markov, G., Sangaa, D., Hirazawa, H. (2018). Structural and Magnetic Properties of Copper Substituted Mg-Ferrites. *EPJ Web of Conferences*, 185, 04010.

Kumar, A., Sharma, P., Varshney, D., (2014). Structural, vibrational and dielectric study of Ni doped spinel Co ferrites: $Co_{1-x}Ni_xFe_2O_4$ (x = 0.0, 0.5, 1.0). *Ceramic International*, 40, 12855-12860.

Kumar, G., Kotnala R.K., Shah, J., Kumar, V., Kumar, A., Dhimana, P., Singh, M. (2017). Cation distribution a key to ascertain the magnetic interactions in cobalt substituted Mg-Mn nanoferrite matrix. *Physical Chemistry Chemical Physics*, 19, 16669.

Kumar, L., Kumar, P. Amarendra Narayan, Manoranjan Kar. (2013). Rietveld analysis of XRD patterns of different sizes of nanocrystalline cobalt ferrite. International Nano Letters, 3, 8.

Mamiya, H. (2013). Hyperthermic effects of dissipative structures of magnetic nanoparticles in large alternating magnetic fields. *Journal of Nanomaterials*, 2013, 1-17.

Mozafari, M., Hadadian,Y., Aftabi, A., Moakhar, M.O. (2014). The effect of cobalt substitution on magnetic hardening of magnetite. *Journal of Magnetism and Magnetic Materials*, 354, 119-124.

O'Handley, R.C. (2000). Modern Magnetic Materials Principles and Applications; Wiley: New York. p.768

Plyasova, L.M., Minyukova, T.P. (2018). Cation distribution in $CuFe_{2-x}Cr_xO_4$ spinels studied by neutron diffraction and its effect on catalytic properties in water gas shift reaction. *Materials Chemistry and Physics*, 211, 278-282.

Rosensweig, R. (2002). Heating magnetic fluid with alternating magnetic field. *Journal of Magnetism and Magnetic Materials*, 252, 970.

Sabri, K., Rais, A., Taibi, K., Moreau, M., Ouddane, B., Addou, A. (2016). Structural Rietveld refinement and vibrational study of $MgCr_xFe_{2-x}O_4$ spinel ferrites. *Physica B: Condensed Matter*, 501, 38-44.

Sirinavas, Ch., Tirupanyam, B.V., Meena, S.S. (2016). Structural and magnetic characterization of co-precipitated $Ni_xZn_{1-x}Fe_2O_4$ ferrite nanoparticles. *Journal of Magnetism and Magnetic Materials*, 407, 135-141.

Vallejo-Fernandez, G., et al., (2013). Mechanisms of hyperthermia in magnetic nanoparticles. *Journal of Physics D: Applied Physics*, 46, 31, 312001.

Watawe, S.C., Sutar, B.D. (2001). Infrared studies of some mixed Li–Co ferrites. *International Journal of Inorganic Materials*, 3, 7, 819–823.

Young, R.A., Wiles, D.B. (1982). Profile Shape Functions in Rietveld Refinements. *Journal of Applied Crystallography*, 15, 430-438.

Zaki, H.M., Dawoud, H.A. (2010). Far-infrared spectra for copper–zinc mixed ferrites. *Physica B: Condensed Matter*, 405, 4476-4479.